2-2009

Integration Host Factor (IHF) Dictates the Structure of Polyamine-DNA Condensates: Implications for the Role of IHF in the Compaction of Bacterial Chromatin

Ishita Mukerji
Wesleyan University, imukerji@wesleyan.edu

Integration Host Factor (IHF) Dictates the Structure of Polyamine-DNA Condensates: Implications for the Role of IHF in the Compaction of Bacterial Chromatin†

Tumpa Sarkar,‡,§ Anton S. Petrov,§,|| Jason R. Vitko,⊥ Catherine T. Santai,‡,§ Stephen C. Harvey,§,|| Ishita Mukerji,⊥ and Nicholas V. Hud*,‡,§

School of Chemistry and Biochemistry, Petit Institute of Bioengineering and Bioscience, and School of Biology, Georgia Institute of Technology, Atlanta, Georgia 30332, and Molecular Biology and Biochemistry Department, Molecular Biophysics Program, Wesleyan University, Middletown, Connecticut 06459

Received October 26, 2008

ABSTRACT: Integration host factor (IHF), a nucleoid-associated protein in bacterial cells, is implicated in a number of chromosomal functions including DNA compaction. IHF binds to all duplex DNA with micromolar affinity and at sequence-specific sites with much higher affinity. IHF is known to induce sharp bends in the helical axis of DNA in both modes of binding, but the role of IHF in controlling DNA condensation within bacterial cells has remained undetermined. Here we demonstrate that IHF influences the morphology of DNA condensed by polyamines in vitro. In the absence of IHF, spermidine and spermine condense DNA primarily into toroidal structures, whereas in the presence of IHF, polyamines condense DNA primarily into rodlike structures. Computer simulations of DNA condensation in the absence and presence of IHF binding lend support to our model in which DNA bending proteins, such as IHF and HU, promote the condensation of DNA into rodlike structures by providing the free energy necessary to bend DNA at the ends of linear bundles of condensed DNA. We propose that a common function of IHF and HU in bacterial cells is to facilitate DNA organization in the nucleoid by the introduction of sharp bends in chromosomal DNA.

DNA condensation is of fundamental importance to all biological organisms (*1*). In bacteria, the genome is highly condensed in a structure called nucleoid. Although the detailed organization of the chromosome in the bacterial nucleoid remains elusive, it is known that DNA condensation is mediated by the combined effects of several factors, including DNA supercoiling, nucleoid-associated proteins, polyamines, and macromolecular crowding effects (*2*−*8*). DNA within the nucleoid is organized and condensed at multiple levels. In *Escherichia coli*, for example, the 4.7 Mb circular chromosome is organized into multiple topologically independent domains that that are approximately 10 kb in size (*9*−*14*). DNA within these domains is negatively supercoiled, with approximately half of the supercoils being interwound and highly branched structures, which significantly compacts the DNA within the nucleoid (*15, 16*). The major nucleoid-associated proteins further package the chromosomal DNA into a more condensed structure.

Among these nucleoid-associated proteins, IHF and HU are called architectural proteins because they induce pronounced bends in DNA upon binding. Kinks in the DNA helix are introduced through the intercalation of proline residues between DNA bases (*17*). IHF and HU are 40% homologous in sequence, and the overall fold of IHF is almost identical to that of HU (*17*−*21*). Interestingly, despite the similarities in structure, HU shows little sequence specificity in DNA binding and a low affinity for linear DNA, whereas IHF binds to specific DNA sequences with nanomolar affinity. The ability of IHF to bend DNA upon sequence-specific binding is central to its currently identified cellular functions, including replication, transposition, regulation of transcription initiation, site-specific recombination of λ phage, and packaging of phage DNA (*22*−*25*). A typical sequence-specific IHF binding site is 30−35 bp in length, which contains a 13 bp consensus sequence, WATCAANNNNTTR (W is A/T, R is G/A, and N is any base) (*26*). In addition to binding sequence-specific DNA sites, IHF also binds to DNA in a sequence-independent manner, but with 10^3−10^4-fold lower affinity, and can be substituted with HU at non-sequence-specific sites (*25, 27, 28*).

IHF is a highly abundant protein whose intracellular concentration varies with growth phase (*29, 30*). The total intracellular concentration of IHF in *E. coli* cells is estimated to vary between 6000 dimers per cell in the exponential phase to 30000 dimers per cell in the stationary phase (*30*). In contrast, the intracellular concentration of free IHF is experimentally determined to be 15−35 nM (*27*). Since there are only a few hundred specific IHF binding sites per *E. coli* choromosome (*31, 32*), the majority of IHF molecules

† This work was supported by the National Institutes of Health (Grants GM62873 to N.V.H. and GM70785 to S.C.H.), the National Science Foundation (Grant MCB-0316625 to I.M.), fellowship funds from the Howard Hughes Medical Institute (J.R.V.), and the U.S. Department of Education's Graduate Assistance in Areas of National Need (C.T.S.).

* To whom correspondence should be addressed. Telephone: (404) 385-1162. Fax: (404) 894-2295. E-mail: hud@chemistry.gatech.edu.
‡ School of Chemistry and Biochemistry, Georgia Institute of Technology.
§ Petit Institute of Bioengineering and Bioscience, Georgia Institute of Technology.
|| School of Biology, Georgia Institute of Technology.
⊥ Wesleyan University.

10.1021/bi8019965 CCC: $40.75
Published on Web 01/08/2009

(6−30 μM) are suggested to be nonspecifically bound to chromosomal DNA. This implies that nonspecific binding by IHF may have important biological functions (*27*). Recent single-molecule experiments have shown that IHF induces a mere ~30% compaction of DNA by binding to multiple sequence-independent low-affinity sites which suggest a role of IHF protein in bacterial chromosome packaging (*33*).

In addition to DNA supercoiling and nucleoid-associated proteins, molecular crowding and polyamines also play a critical role in bacterial chromosome condensation, dictating the well-defined volume of the nucleoid mass (*5, 7, 34*−*38*). Cellular polyamines, which are polycationic at physiological pH, are important components of bacterial cells and also well-characterized DNA condensing agents (*39, 40*). In prokaryotes, the most abundant polyamines are putresciene and spermidine (*41*−*43*). The high cellular abundance of these polyamines (5−20 mM) and the ability of spermidine to stabilize the condensed bacterial chromosome in isolated nucleoids suggest an important role of polyamine in the compaction of DNA in bacterial cells (*41, 44*).

Although chromosomal DNA in bacteria is believed to be condensed into the nucleoid by the combined effects described above, no single factor is sufficient for achieving high-density DNA condensation. Zimmerman and co-workers have presented evidence that cellular extracts from *E. coli* can work together with HU to condense DNA (*35, 45*). Subsequent studies suggested that nucleoid-associated proteins are not primarily responsible for maintaining the condensed form of DNA in isolated nucleoids (*38, 46*), but a more recent study from the Record laboratory has clearly shown that HU can either condense or extend DNA, depending on the relative concentration of HU to DNA (*47*). The molecular mechanisms by which nucleoid-associated proteins work with each other, polyamines, macromolecular crowding, and DNA topology to control chromosome condensation have not been systematically explored. Although nucleoid-associated proteins have been implicated in the organization of the *E. coli* chromosome in the nucleoid, their modes of action in vivo are still the source of an ongoing debate. Finally, the direct role of HU in governing DNA morphology in bacteria is strongly illustrated by a recent study by Adhya and co-workers in which a HU double mutant was shown to dramatically alter nucleoid compaction and cell morphology (*48*).

We have recently shown that HU functions as an architectural protein that guides DNA to condense into linear rodlike structures in the presence of polyamines and macromolecular crowding agents but does not act as a condensing agent per se (*49*). On the basis of these observations, we have proposed that HU works in a similar manner in vivo to locally organize and condense the bacterial chromosome. In this work, we performed experiments to elucidate the effect of IHF on DNA condensation. In particular, the focus of this study was to gain insight into the possible interplay among IHF, DNA supercoiling, and polyamines in DNA compaction. Since IHF plays a role in bacterial condensation, a basic understanding of how IHF interacts with DNA in the presence of other cellular factors to initiate DNA condensation is important for obtaining a molecular-level description of condensed DNA within the bacterial nucleoid.

Here we report that IHF, like HU, has a dramatic effect on the morphology of particles produced upon the condensation of DNA. Furthermore, it is shown that IHF has the same effect on condensates produced by a variety of DNA molecules, varying in length and topology (i.e., linear, supercoiled). On the basis of the experimental and computer simulation results presented here, and what was previously known about DNA packaging in bacteria, a model for the organization of DNA within the nucleoid and the contribution of IHF and HU in maintaining this organization is presented.

MATERIALS AND METHODS

DNA Preparation. DNA described in the text as 3.4 kb DNA and 3.9 kb DNA were derived from bacterial plasmid pBluescript II SK− (Stratagene) using standard molecular biology techniques (Supporting Information). The 10.7 kb circular DNA plasmid was the YEp13 yeast episomal vector. λ phage DNA was purchased from Invitrogen.

For experiments that required sequence-specific IHF binding sites, synthetic duplexes containing the H′ site of λ phage (sequence given below), one of the best-characterized and highest-affinity IHF binding sites (*17, 27*), were incorporated into the 3.4 and 3.9 kb plasmids. The consensus sequence for IHF binding is in bold. Plasmids containing one and two specific IHF binding sites were generated for both the 3.4 and 3.9 kb DNA. For the plasmids with two specific IHF binding sites, these sites were separated by 500 bp in the 3.4 kb plasmid and by 950 bp in the 3.9 kb plasmid. The sequences containing the IHF binding site(s) were confirmed by the dideoxy-NTP sequencing method. Plasmids were transformed into appropriate *E. coli* strains (Supporting Information) and isolated using the Qiagen (Valencia, CA) maxi-prep kit. To remove any IHF proteins bound to the plasmids after isolation, purified plasmids containing high-affinity IHF binding sites were treated with proteinase K. Proteinase K was removed by heat inactivation at 65 °C and the Qiagen PCR purification kit. The 3.4 and 3.9 kb plasmids were linearized by digestion with restriction endonuclease *Sca*I, and the 10.7 kb DNA plasmid was linearized by digestion with restriction endonuclease *Bam*HI (New England Biolabs).

```
5'-AGCTTAAAAAAGCATTGCTTATCAATTTGTTGCA-3'
    3'-ATTTTTTCGTAACGAATAGTTAAACAACGTCTAG-5'
```

Following enzymatic digestion, the DNA was rinsed at least five times with 1× TE [10 mM Tris and 1 mM EDTA (pH 7.8)] using a Microcon-YM 30 spin column (Millipore) to remove salts and buffers from the restriction digest. The DNA was finally resuspended from the spin column in 1× TE. The DNA concentration was determined spectrophotometrically. Supercoiled plasmids, obtained directly from the plasmid isolation procedure, were determined to be more than 90% supercoiled on the basis of agarose gel electrophoresis analysis. Supercoiled DNA was also rinsed at least five times with 1× TE to ensure that the buffer conditions of all DNA stock samples were identical.

IHF Protein Isolation. IHF was prepared as previously described (*50*) from an overexpressing HN880 strain (gift from H. Nash and S. Goodman). The DNA binding activity of the isolated protein was determined by the gel mobility shift assay method and found to be consistent with that determined by other laboratories (*51*).

Preparation of DNA Condensates. Spermidine-induced condensates were prepared by mixing solutions of DNA and spermidine to yield a final condensation reaction mixture of 5 μM DNA (in units of base pairs throughout), 700 μM spermidine, 0.33× TE (pH 7.8), and 15 mM KCl. The condensate reaction mixtures were allowed to equilibrate at room temperature for 10 min before being deposited on grids. The same protocol was followed for the preparation of spermine-induced condensates, in which DNA was mixed with spermine to yield a condensation reaction mixture of 5 μM DNA, 15 μM spermine, 0.33× TE (pH 7.8), and 15 mM KCl. For spermidine-induced condensates prepared in the presence of IHF, DNA was incubated with IHF for 10 min and then condensed with spermdine for 10 min before being deposited on grids. All the final condensate solutions contained 5 μM DNA, 700 μM spermidine, 0.33× TE (pH 7.8), and 15 mM KCl. For spermine DNA condensation in the presence of IHF, the same protocol described above for the condensation of DNA by spermidine in the presence of IHF was followed, where all final condensate solutions contained 5 μM DNA, 15 μM spermine, 0.33× TE (pH 7.8), and 15 mM KCl.

Electron Microscopy and Analysis of DNA Condensates. A 10 μL aliquot of each condensate solution was deposited on a carbon-coated EM grid (Ted Pella, Redding, CA), after 15 min stained with 2% uranyl acetate, rinsed with 95% ethanol, and air-dried. Imaging was performed with a JEOL-100C transmission electron microscope (TEM) at a magnification of 100000×. The grid surface was randomly scanned to obtain the relative toroid and rod populations in each sample, and the numbers of unaggregated toroids and rods visible on the viewing screen were counted. Several hundred structures were counted for each grid. Each measurement reported is the average of the counts from three different EM grid preparations. The dimensions of individual condensates for each sample were measured using a computer graphics program.

Computer Simulations. DNA condensation was simulated within the framework of a coarse-grained model containing a linear chain of pseudoatoms (beads), each representing 6 bp and connected by springs; the model was parametrized to mimic the elastic and electrostatic properties of DNA. The parametrization procedure is described in detail elsewhere (*52, 53*). Each simulation contained a single DNA molecule, 567 beads (3.4 kb) in length. The force field accounted for the elastic (stretching and bending) terms described by harmonic potentials, a semiharmonic volume exclusion term and a DNA–DNA interaction term. In the notation of the earlier publications (*52, 53*), numeric values of the harmonic and semiharmonic potentials were as follows: $k_b = 3.5$ kcal mol^{-1} Å^{-2}, $b_0 = 19.9$ Å, $k_\theta = 22.4$ kcal mol^{-1} rad^{-2}), $\theta_0 = \pi$ rad, $k_{DNA-DNA} = 3.5$ kcal mol^{-1} Å^{-2}, and $d_{0,DNA-DNA} = 25.0$ Å.

The interaction between DNA strands is described by empirically derived eq 1:

$$E_{attr}^{DNA-DNA}(r) = A_1\left\{\exp\left[\frac{2(b_1 - r)}{c_1}\right] - 2\exp\left(\frac{b_1 - r}{c_1}\right)\right\} - A_2\left\{\exp\left[\frac{2(b_2 - r)}{c_2}\right] - 2\exp\left(\frac{b_2 - r}{c_2}\right)\right\} \quad (1)$$

where $A_1 = 11$ cal mol^{-1} bp^{-1}, $A_2 = 12$ cal mol^{-1} bp^{-1}, $b_1 = 30.5$ Å, $b_2 = 37.5$ Å, $c_1 = 2.6$ Å, and $c_2 = 2.2$ Å. The parameters have been derived to match the data for the attractive regime in the range of ∼25−34 Å with a minimum of ∼130 cal mol^{-1} bp^{-1} at ∼27.2 Å (*54*) and the repulsive Debye−Hückel regime in the range of 35−50 Å, based on experimental results from DNA compression by osmotic pressure obtained by Rau and Parsegian (*55*).

The net effect of IHF binding, which promotes DNA bending, was modeled by introducing 15 flexible sites along the DNA. These flexible sites, for which bending constants were reduced by a factor of 100 from the original values, i.e., $k'_\theta = 0.224$ kcal mol^{-1} rad^{-2}), were randomly placed along the DNA molecules by sampling from a uniform probability distribution.

Two series of 50 simulations containing DNA molecules in different starting configurations with and without flexible sites were performed. Starting configurations were generated by running a MD trajectory for a single free DNA with the repulsive potential without extra sites of flexibility, as described previously (*53*), using a MD time step of 0.5 ps and saving conformations every 2×10^6 steps.

A total of 5×10^6 steps of MD for each DNA in the attractive regime with and without flexible sites were performed with a time step of 0.5 ps. All systems were coupled to a Berendsen thermostat (*56*) with a coupling time constant of 250 ps. Coordinates were saved every 5000 steps along each MD trajectory. All MD simulations were performed using the YUP package, designed for simulations of coarse-grained and low-resolution models (*57*).

RESULTS

IHF Governs the Morphology of Spermidine Condensates Formed from Linear DNA. The polyamine spermidine is known to cause the condensation of DNA in vitro and is implicated in maintaining the condensed state of DNA within bacteria. Thus, as a means of exploring the effects of IHF on DNA condensation, we performed in vitro condensation studies with spermidine in the presence of IHF. Linear DNA molecules of different lengths (3.4, 10.7, and 48.5 kb) were preincubated with IHF protein, then condensed with spermidine, and examined using electron microscopy. It is well documented that condensation of DNA with a length of >2 kb by spermidine from aqueous solution results in primarily toroidal structures, with a small percentage of rodlike structures (<10%) (*40, 58−60*). As illustrated by the EM images shown in Figure 1, if DNA is preincubated with IHF prior to condensation by spermidine, a significant increase is observed in the population of rodlike condensates.

A plot of relative rod and toroid condensate populations as a function of IHF concentration provides a quantitative illustration of the increase in the relative rod population with an increase in IHF concentration (Figure 2). For spermidine-induced condensation of 3.4 kb linear DNA, the relative population of rodlike condensates increases from <5% rods (in the absence of IHF) to >90% rods in the presence of 75 nM IHF, with the half-maximal rod population being observed at 34 nM (Figure 2A). For longer DNA, such as 10.7 kb plasmid or 48.5 kb λ phage DNA, a similar magnitude increase in relative rod populations was observed as a function of IHF concentration. These results demonstrate that the effect of IHF on DNA condensation is independent of DNA length (Figure 2A).

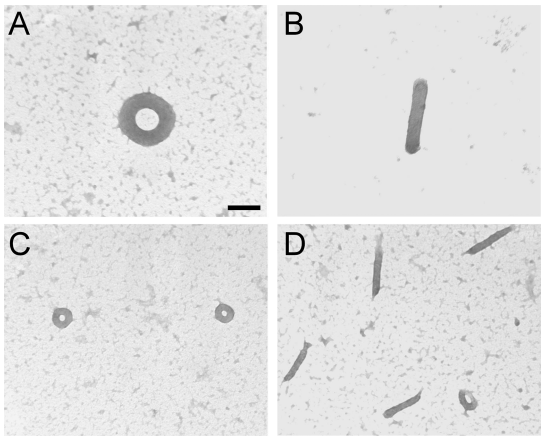

FIGURE 1: Transmission electron microscopy (TEM) images of polyamine-induced linear DNA condensates produced in the presence and absence of IHF. (A) DNA condensate produced by the addition of spermidine to linear 3.4 kb DNA. (B) DNA condensate produced by the addition of spermidine to linear 3.4 kb DNA in the presence of 75 nM IHF. (C) DNA condensates produced by the addition of spermine to linear 3.4 kb DNA. (D) DNA condensates produced by the addition of spermine to linear 3.4 kb DNA in the presence of 125 nM IHF. All reaction mixtures contained the following final concentrations: 5 μM DNA base pairs, 700 μM spermidine chloride or 15 μM spermine chloride, 0.33× TE (pH 7.8), and 15 mM KCl. The scale bar is 100 nm.

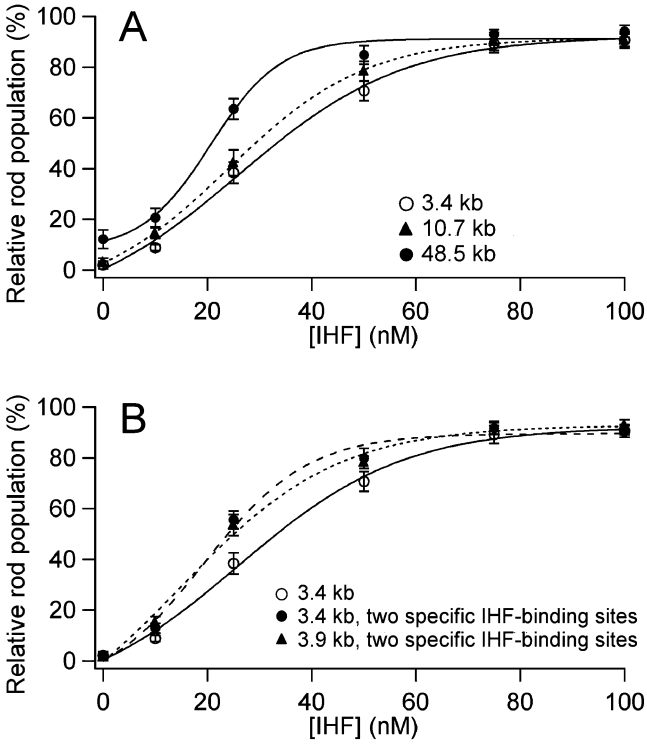

FIGURE 2: Spermidine-induced DNA condensate morphology statistics as a function of IHF concentration for (A) linear DNA and (B) linear plasmid DNA incorporated with specific IHF-binding sites. All reaction mixtures contained the following final concentrations: 5 μM DNA base pairs, 700 μM spermidine chloride, 0.33× TE (pH 7.8), 15 mM KCl, and the indicated concentrations of IHF dimer. Each rod population measurement reported is the average of several hundred counts from three different EM grid preparations. Curves are sigmoidal least-squares fits of experimental data. Error bars indicate standard deviations of measurements.

DNA rods produced by spermidine-induced condensation of 3.4 kb DNA in the presence of IHF exhibited an overall mean length of 383 nm and a mean width of 57 nm at an IHF concentration of 75 nM (Table 1). Rod length and thickness proved to be relatively insensitive to IHF concentration at the point where the relative rod population almost reaches a plateau. For example, rods formed in the presence of 100 nM IHF had a mean length of 375 nm (σ, ±28 nm) and a mean thickness of 55 nm (σ, ±10 nm). These observations demonstrate that IHF does not significantly alter the dimensions of rods and toroids produced by spermidine, only the relative population of rods and toroids. We also note that spermidine−DNA rodlike condensates formed from DNA of different lengths (3.4, 10.7, and 48.5 kb) in the presence of 75 nM IHF have very similar dimensions (Table 1).

Table 1: Dimensions of Rodlike DNA Condensates Formed in the Presence of IHF Protein[a]

Linear DNA

DNA length (kb)	condensing agent	length (nm)	thickness (nm)
3.4	spermidine	383 (σ, ±32)	57 (σ, ±8)
10.7	spermidine	406 (σ, ±27)	59 (σ, ±9)
48.5	spermidine	396 (σ, ±36)	58 (σ, ±9)
3.4	spermine	206 (σ, ±35)	34 (σ, ±3)
10.7	spermine	231 (σ, ±31)	32 (σ, ±5)
48.5	spermine	248 (σ, ±32)	30 (σ, ±3)

Supercoiled DNA

DNA length (kb)	condensing agent	length (nm)	thickness (nm)
3.4	spermidine	352 (σ, ± 41)	51 (σ, ±7)
10.7	spermidine	375 (σ, ± 40)	50 (σ, ±8)
3.4	spermine	206 (σ, ± 35)	32 (σ, ±6)
10.7	spermine	231 (σ, ± 32)	35 (σ, ±4)

Linear DNA with One or Two Specific IHF-Binding Sites

DNA length (kb)	IHF sites	condensing agent	length (nm)	thickness (nm)
3.4	one	spermidine	373 (σ, ±24)	56 (σ, ±8)
3.4	two, 500 bp apart	spermidine	394 (σ, ±33)	58 (σ, ±9)
3.9	one	spermidine	391 (σ, ±25)	57 (σ, ±11)
3.9	two, 950 bp apart	spermidine	373 (σ, ±46)	57 (σ, ±7)
3.4	one	spermine	227 (σ, ±29)	31 (σ, ±4)
3.4	two, 500 bp apart	spermine	203 (σ, ±26)	34 (σ, ±5)
3.9	one	spermine	212 (σ, ±32)	30 (σ, ±9)
3.9	two, 950 bp apart	spermine	202 (σ, ±24)	34 (σ, ±7)

Supercoiled DNA with Two Sequence-Specific IHF-Binding Sites

DNA length (kb)	condensing agent	length (nm)	thickness (nm)
3.4	spermidine	340 (σ, ±43)	48 (σ, ±8)
3.4	spermine	200 (σ, ±27)	34 (σ, ±5)

[a] For all samples, DNA was 5 μM in base pairs. For spermidine samples, spermidine was 700 μM and IHF 125 nM. For spermine samples, spermine was 15 μM and IHF 75 nM. Several hundred measurements were taken from each sample, and from three different EM grid preparations. Variations in measurements indicate standard deviations. See Materials and Methods for additional details.

IHF Governs the Morphology of Spermine Condensates of Linear DNA. Linear DNA 3.4, 10.7, and 48 kb in length was condensed with the tetracationic polyamine, spermine, in the absence and presence of IHF. Similar to the spermidine results presented in the previous section, when linear DNA was condensed by spermine the majority of particles formed (>95%) were well-defined toroids with a minor population of rods (Figure 1C). DNA that was condensed by spermine in the presence of 125 nM IHF also exhibited a striking increase in the percentage of rodlike condensates, approximately 85% as compared to <5% in the absence of IHF (Figure 1D). These results demonstrate that guiding

DNA condensate morphology is a general property of IHF, rather than a property that is particular to either spermidine- or spermine-induced condensates. We note that a higher concentration of IHF was required to produce a majority of rodlike spermine−DNA condensates, as compared to spermidine−DNA condensates. The origin of this difference in required IHF concentration has not yet been determined but may be a result of the different charges of spermine (4+) and spermidine (3+). HU exhibits a very similar polyamine-dependent concentration for controlling condensate morphology (*49*).

In contrast to the condensates formed in the presence of spermidine, the condensates formed by spermine are considerably smaller (Figure 1). For example, toroids formed upon the condensation of linear 3.4 kb DNA by spermine had a mean outside diameter of 97 nm (σ, ±6 nm) and a mean thickness of 38 nm (σ, ±3 nm). The overall dimensions of the spermine−DNA rodlike condensates formed in the presence of 125 nM IHF were also considerably smaller than those produced by spermidine (Table 1). The mean length of spermine−DNA rods formed from linear 3.4 kb DNA in the presence of IHF was 206 nm (σ, ±35 nm) and the mean rod thickness 34 nm (σ, ±3 nm), compared to 383 nm (σ, ±32 nm) and 57 nm (σ, ±8 nm), respectively, for the same DNA condensed by spermidine in the presence of IHF (Table 1).

The dimensions of spermine-induced rodlike condensates formed in the presence of IHF did not vary significantly with DNA length. The rods formed by linear 3.4 kb DNA in the presence of 125 nM IHF exhibited a mean length of 206 nm (σ, ±35 nm) and a mean thickness of 34 nm (σ, ±3 nm), while under similar conditions, rods formed by 10.7 and 48.5 kb DNA exhibited mean lengths of 231 nm (σ, ±31 nm) and 248 nm (σ, ±32 nm), respectively, and mean thicknesses of 32 nm (σ, ±5 nm) and 30 nm (σ, ±3 nm), respectively (Table 1). These results also suggest a purely architectural role of IHF in DNA condensation. That is, IHF exhibits a similar effect on the morphology of DNA condenstes in a manner independent of condensing agent structure and DNA length.

IHF Governs the Morphology of Supercoiled DNA That Models Various Domain Sizes. We have also investigated the effects of IHF on the condensation of supercoiled DNA by polyamines. Supercoiled DNA is the natural substrate of IHF in bacterial cells, and supercoiling of DNA within topologically independent domains (~10 kb in average size) facilitates bacterial chromosome compaction in vivo (*14, 61*). We investigated spermidine-induced condensation of 3.4 and 10.7 kb supercoiled DNA. The condensation of supercoiled DNA by spermidine (in the absence of IHF) produces approximately 40% rods and 60% toroids (Figure 3A). The greater population of rods observed upon the condensation of supercoiled DNA, as compared to linear DNA, has been discussed in previous reports (*49*). The incubation of supercoiled DNA with 75 nM IHF before condensation with spermidine resulted in an increase in the population of rods to >95% (Figure 3B). The spermidine-induced rods formed by the condensation of 3.4 and 10.7 kb supercoiled DNA in the presence of IHF had similar dimensions (Table 1).

Condensation of the 3.4 and 10.7 kb supercoiled DNA by spermine (in the absence of IHF) also produced a mixture of toroids and rods (i.e., 55% toroids and 45% rods). When supercoiled DNA was condensed by spermine in the presence of 125 nM IHF, an increase in the relative rod populations to >90% was observed for both DNA molecules (Figure 3). The rodlike condensates formed by spermine in the presence of IHF were approximately 200 nm in length and 30 nm in thickness. Rod dimensions did not change significantly with the length of the supercoiled DNA (Table 1). In contrast, significant differences in condensate dimensions were observed for the trivalent spermidine versus the tetravalent spermine (Table 1). These results illustrate that the effects of IHF on DNA condensation are similar for linear and supercoiled DNA. Our findings also demonstrate that supercoiled DNA is compacted by polyamines into linear bundles in the presence of IHF proteins, with bundle length being dictated mostly by the nature of the condensing agent rather than DNA length.

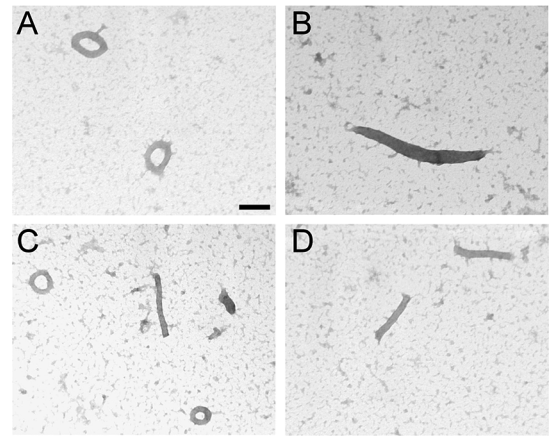

FIGURE 3: Transmission electron microscopy (TEM) images of polyamine-induced supercoiled DNA condensates produced in the presence and absence of IHF. (A) DNA condensate produced by the addition of spermidine to 3.4 kb supercoiled DNA. (B) DNA condensate produced by the addition of spermidine to 3.4 kb supercoiled DNA in the presence of 75 nM IHF. (C) DNA condensates produced by the addition of spermine to 3.4 kb supercoiled DNA. (D) DNA condensates produced by the addition of spermine to 3.4 kb supercoiled DNA in the presence of 125 nM IHF. All reaction mixtures contained the following final concentrations: 5 μM DNA base pairs, 700 μM spermidine chloride or 15 μM spermine chloride, 0.33× TE (pH 7.8), and 15 mM KCl. The scale bar is 100 nm.

Nonspecific Binding by IHF Principally Governs DNA Condensate Morphology. A number of DNA sequences to which IHF binds more tightly as compared to most other DNA sequences have been identified (*25*−*28*). There are no apparent specific binding sites for IHF along the 3.4 kb plasmid DNA. Therefore, it was of interest to determine if specific IHF binding sites produce additional effects on the structure or size of DNA condensates or at the concentration of IHF required to promote the formation of rodlike condensates. With this goal, one and two specific IHF binding sequences were introduced into plasmid DNA. To also examine if the distance between two IHF sites affected DNA condensation, two specific IHF sites were incorporated 500 and 950 bp apart. These modified plasmid DNA molecules were preincubated with IHF protein and then condensed by spermidine.

The 3.4 and 3.9 kb linear DNA containing only one specific IHF binding site, and 10.7 kb linear plasmid DNA (which contains one natural IHF-specific site), were condensed by spermidine in the presence of 75 nM IHF and found to produce rod populations that were >90% in all

cases. The dimensions of the rodlike condensates formed from these DNA samples were very similar to those of the condensates reported above, under the same experimental conditions (Table 1). Thus, the dramatic increase in the relative rod population and similar dimensions for spermidine−DNA condensates formed in the presence of IHF for 3.4−48.5 kb linear DNA, with and without IHF-specific sites, demonstrate the general ability of IHF to guide condensation irrespective of the presence of IHF-specific binding sites.

A definite shift in the DNA condensate morphology from toroid to rod was again observed with an increase in IHF concentration for spermidine−DNA condensates, irrespective of whether IHF-specific sites were present in the DNA (Figure 2). The similar magnitude increase in relative rod populations of linear DNA molecules with specific IHF-binding sites and without specific sites, as a function of IHF concentration, indicates that the effect of IHF on DNA condensation is due to the non-sequence-specific binding of IHF to the DNA (Figure 2). However, we note that the introduction of sequence-specific IHF-binding sites does appear to slightly reduce the IHF concentration required to produce rodlike condensates. In particular, for 3.4 kb linear DNA containing no sequence-specific IHF-binding sites, an IHF dimer concentration of 34 nM was required for the half-maximal rod population for spermine−DNA condensates, whereas this concentration is apparently reduced to approximately 25 nM for both 3.4 kb linear DNA containing two specific IHF sites and 3.9 kb linear DNA containing two specific IHF sites (Figure 2B).

The dimensions of the spermidine-induced rod condensates formed in presence of 75 nM IHF, where relative rod populations were >90% for all linear DNA mentioned above, are listed in Table 1. Rodlike condensates were similar in size for 3.4 kb linear DNA containing no IHF-specific sites, 3.4 kb linear DNA containing two specific IHF binding sites 500 bp apart, and 3.9 kb linear DNA containing two specific IHF binding sites 950 bp apart.

The dimensions of spermine−DNA rods were also found to be insensitive to the presence of specific IHF-binding sites (Table 1). Similar results were obtained when supercoiled DNA with two specific IHF-binding sites was condensed by spermidine or spermine under the same experimental conditions as linear DNA. Rod dimensions did not change significantly with the length of the supercoiled DNA or with the introduction of specific IHF-binding sites (Table 1).

Computer Simulations of DNA Condensation in the Absence and Presence of IHF. The observations presented here with regard to the influence of IHF on DNA condensation, and in our previous study with HU (*49*), cleary demonstrate that DNA-bending proteins strongly promote the formation of rodlike condensates over toroidal condensates. We have previously proposed that DNA-bending proteins exert this influence on condensate morphology by providing some of the free energy required for the sharp bends at the ends of rods. Additionally, in a different study regarding the relative populations of toroidal and rodlike condensates, in the absence of bound proteins, we provided evidence that the free energy required to smoothly bend the DNA throughout a toroid is roughly equivalent to the free energy required to produce the sharp, discrete bends necessary for a rodlike condensate (*62*). In that study, we demonstrated that the introduction of one static DNA loop (i.e., 300 bp of sequence-directed curvature) per 3.4 kb of plasmid DNA was sufficient to increase the relative toroid population from ~70% (30% rods) to ~90% (10% rods) (*62*).

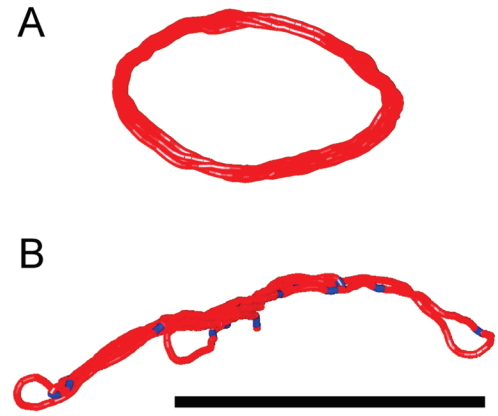

FIGURE 4: Conformations of 3.4 kb condensed DNA molecules from MD simulations. The same initial conformation leads to the toroidal (A) and rodlike (B) structures, when the simulations are conducted in the elastic (no IHF) and flexible (with IHF) regimes, respectively. Flexible sites are colored blue. Although not obvious from the figure, the flexible sites are preferentially associated with loop regions, as discussed in the text. The scale bar is 100 nm.

Given the observed influence of IHF and HU on the morphology of DNA condensates, we hypothesize that the introduction of a few highly flexible sites per DNA plasmid (from bound IHF or HU proteins) should significantly shift the relative population of toroids and rods to more rods, even if only a fraction of the 180° bends within a rod contained a highly flexible site. As a means of exploring the validity of this proposal and potentially explaining the influence of IHF and HU on DNA condensate morphology, we have conducted computer simulations of DNA condensation in which flexible sites, representing bound IHF or HU, were introducted into otherwise semirigid DNA polymers prior to simulated condensation.

Course-grained models were developed to represent the condensation of 3.4 kb DNA in the absence and presence of DNA-bending proteins (Materials and Methods). Fifty initial conformations were generated for use in two sets of DNA condensation simulations, for a total of 100 simulations. In the first set, all DNA segments were parametrized with the same bending energy to represent DNA condensation in the absence of DNA-bending proteins. In the second set, 15 flexible segments were randomly distributed along each of the 50 initial DNA models to represent plasmids with DNA-bending proteins bound at a density of one protein per 225 bp, a density which corresponds to the lowest density of HU required to cause the majority of DNA condensates to have a rodlike morphology (*49*).

Without the flexible sites, 26 of 50 condensation simulations produced toroids, with the remaing 24 simulations producing rods (i.e., 48% rods). With the flexible sites introduced, these numbers are 13 toroids and 37 rods (i.e., 74% rods). In Figure 4, a pair of condensed structures that resulted from the same starting DNA conformation is shown, with DNA in one simulation containing no bound proteins [i.e., without highly flexible sites (Figure 4A)] and the second with 15 randomly distributed flexible sites [colored blue (Figure 4B)]. The Supporting Information contains movies for a pair of representative condensation trajectories for a

DNA plasmid condensed from the same initial conformation state, with and without flexible regions.

A detailed analysis of the 37 rods produced from the model DNA plasmids with flexible sites revealed that the sharp bends within these rods, on average, constitute approximately 20% of the total length of the DNA molecule. If the distribution of these bends along the DNA were uncorrelated with the positions of the flexible sites, one would expect the sharp bends to contain, on average, ~3 of 15 flexible sites (i.e., 20%). The analysis indicated that the sharp bends contain, on average, 6.2 of 15 flexible sites (i.e., 41%). This greater concentration of flexible sites in the sharply bent regions supports a positive correlation between the presence of a flexible site and the probability that DNA will fold back to form a rod during condensation. A histogram of the average number of flexible sites within the sharp bends of rods also reveals that of the 37 rods formed from DNA with highly flexible sites, only two rods have three or fewer flexible sites within their sharply bent regions (Supporting Information). The sharp bends within rods contained, on average, 1.15 flexible sites per bend. We note that these flexible sites do not typically make the full 180° bend (Figure 4B), but they do relieve some of the bending strain associated with formation of a sharp bend. This observation also fits well with our proposal that DNA-bending proteins promote the formation of rodlike condensates even if only a portion of the bending energy is provided by protein binding.

DISCUSSION

A Model for Formation of Enhanced Rodlike DNA Condensates in the Presence of IHF. The most obvious difference between DNA condensed in toroids and rods is that the DNA within toroids is smoothly and continuously bent, whereas the DNA within rods contains abrupt bends that are separated by linear regions. The coexistence of rods and toroids as the products of many condensation reactions indicates that the energy required for the smooth bending of the DNA within toroids is almost equal to the energy required for the sharp bends at the end of the rods (*62, 63*). Accordingly, DNA condensation under conditions that make base pair destacking and helix kinking less energetically unfavorable (e.g., in mixed alcohol/water solvents, hydrophobic ligands, and superhelical stress) increases the population of rodlike condensates by lowering the energetic penalty associated with sharp bends (*64*−*69*). Thus, the bends created by IHF in DNA (or spontaneous bends trapped by IHF binding) should be expected to promote rod formation during condensation. In contrast, DNA condensed within toroids is smoothly bent over a radius of curvature that is much greater than that of the sharp bends induced by IHF. Therefore, IHF should not be expected to promote toroid formation. Our computer simulations of DNA condensation with bound IHF (represented by a locally reduced bending energy) at a relatively small number of sites along a DNA plasmid are fully supportive of this model.

We previously demonstrated that HU alone does not condense DNA into densely packed particles but kinetically and thermodynamically stabilizes rodlike DNA condensate structures by acting as a DNA-bending protein during in vitro DNA condensation (*49*). The experiments presented in this study for IHF confirm and extend these conclusions for these

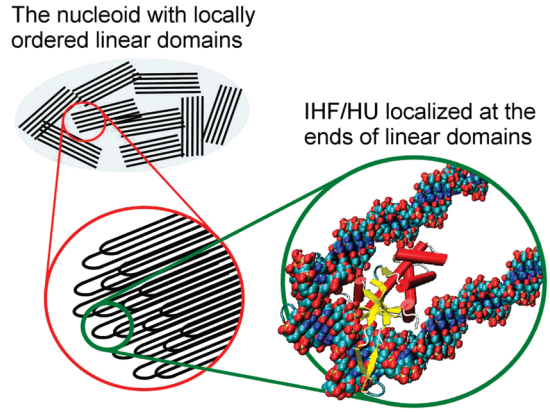

FIGURE 5: Model for a particular mode by which IHF and HU could facilitate DNA packaging and organization within the bacterial nucleoid.

two nucleoid-associated proteins. We have demonstrated that IHF can guide the condensation of DNA into structures with linear bundles (i.e., rods) when DNA is condensed by two different condensing agents, the trivalent spermidine and the tetracationic spermine. Thus, the ability to control DNA condensate morphology appears also to be an intrinsic property of IHF. Together, our results suggest that the primary function of IHF and HU in DNA compaction appears to be architectural in nature.

A Model for the Role of HU and IHF in Bacterial Chromosome Organization. A primary goal of our DNA condensation studies with IHF and HU is to provide insight into the functionality of these DNA-bending proteins in compacting bacterial chromosomes. Here we have shown that IHF strongly influences condensate morphology when DNA is condensed by polyamines, independent of DNA length over the range of 3.5−48.5 kb for linear and supercoiled DNA. The similar effects of IHF and HU on DNA condensation suggest that both proteins have related functions in the modulation of chromosome structure in bacteria. On the basis of these results, we propose that HU and IHF function as architectural proteins during bacterial chromosome condensation by directing the local packing of DNA into a linear bundlelike state.

Our results regarding the effects of HU and IHF on DNA condensation also suggest a possible mode for the action of these proteins in chromosome organization in the bacterial nucleoid (Figure 5). It has been shown that the chromosome is compacted in part by isolated topological domains that are further folded by negative supercoiling (*5, 14, 70*), and that the size of the domains would be dictated by the dynamic domain barriers (*4, 71*). In the presence of polyamines and macromolecular crowding agents (RNA and proteins present in the cytoplasm), DNA helices within these domains approach each other with parallel helix alignment to maximize attractive interactions (i.e., condensation) (Figure 5). In support of this model, the linear arrangement of DNA in the condensed state within bacteria has been revealed by electron microscopy (*72*−*74*). We propose that the binding of DNA helix-bending proteins, including HU and IHF, facilitates linear bundle formation by reducing the free energy required for DNA bending at ends of regions that contain linear regions of condensed DNA (Figure 5). The sequence-independent binding of these proteins would allow them to function throughout the chromosome. Alternatively, it is possible that mulitiple IHF-

specific sites in proper phase along a bacterial chromosome could provide a means by which the start and ends of linear domains are controlled in vivo.

Cellular RNA content could also affect nucleoid condensation by modulating the availability of polyamines for DNA binding, as strong competition between RNA and DNA has been reported for polyamine binding (*46, 75*). In the late stationary phase when most of the DNA binding proteins are degraded, the only proteins present in high copy numbers are Dps (150000 per cell) and IHF (15000 per cell), and also HU (7500 per cell) (*5, 30*). The bacterial chromatin reorganizes into cholesteric crystalline morphologies in which DNA filaments are arranged into local parallel bundle fashion (*73, 74, 76*−*78*). Although the phase transition has been attributed to formation of the DNA−Dps complex (*76, 77, 79*), according to our model other DNA-bending proteins like IHF and HU could also facilitate reorganization of DNA into parallel bundlelike structures in the presence of polyamines. Our model is also consistent with the observation that in starved *dps*$^-$ bacteria the chromosome still organizes into a cholesteric phase (*76, 77*).

The model we have proposed is structurally similar to a model proposed by Zimmerman for DNA organization in the bacterial nucleoid during the growth phase, even though the two models are based upon different observations (*46*). Both models suggest the formation of parallel bundles of condensed DNA, with nucleoid-associated proteins bound at the ends of the bundles. However, Zimmerman proposed that DNA-associated proteins or RNA-polymerase antagonizes DNA condensation and thereby creates loops of DNA that are outside of the linear bundle regions. In contrast, the results presented in our studies of IHF and HU have revealed that these DNA-associated proteins could facilitate formation of parallel DNA bundles. Finally, we note that our condensation experiments, in the absence of any restricted domain barriers, showed that the linear DNA condensate size is independent of DNA length and is controlled by the condensing solution conditions. The scenario could be different during bacterial chromosome compaction in the presence of cellular factors responsible for creating domain boundaries and hence dictating the size of the domains.

ACKNOWLEDGMENT

We thank Gary Newman of the Georgia Institute of Technology for the gift of DNA plasmids. We thank the Georgia Institute of Technology Electron Microscopy Center for use of the JEOL-100C instrument and Ms. Yolande Berta for technical assistance.

SUPPORTING INFORMATION AVAILABLE

Additional details on DNA plasmid construction, sample videos of condensation simultations, and analysis of simulations. This material is available free of charge via the Internet at http://pubs.acs.org.

REFERENCES

1. van Holde, K. (1989) *Chromatin*, Springer-Verlag, New York.
2. Pettijohn, D. E. (1988) Histone-like proteins and bacterial chromosome structure. *J. Biol. Chem. 263*, 12793–12796.
3. Schmid, M. B. (1988) Structure and function of the bacterial chromosome. *Trends Biochem. Sci. 13*, 131–135.
4. Travers, A., and Muskhelishvili, G. (2005) Bacterial chromatin. *Curr. Opin. Genet. Dev. 15*, 507–514.
5. Johnson, R. C., Johnson, L. M., Schmidt, J. W., and Gardner, J. F. (2005) Major nucleoid proteins in the structure and function of the *Escherichia coli* chromosome. In *The Bacterial Chromosome* (Higgins, N. P., Ed.) pp 65−132, ASM Press, Washington, DC.
6. Dame, R. T. (2005) The role of nucleoid-associated proteins in the organization and compaction of bacterial chromatin. *Mol. Microbiol. 56*, 858–870.
7. Stavans, J., and Oppenheim, A. (2006) DNA-protein interactions and bacterial chromosome architecture. *Phys. Biol. 3*, R1−R10.
8. Luijsterburg, M. S., Noom, M. C., Wuite, G. J. L., and Dame, R. T. (2006) The architectural role of nucleoid-associated proteins in the organization of bacterial chromatin: A molecular perspective. *J. Struct. Biol. 156*, 262–272.
9. Worcel, A., and Burgi, E. (1972) Structure of folded chromosome of *Escherichia coli*. *J. Mol. Biol. 71*, 127–147.
10. Delius, H., and Worcel, A. (1974) Electron-microscopic visualization of folded chromosome of *Escherichia coli*. *J. Mol. Biol. 82*, 107–109.
11. Kavenoff, R., and Bowen, B. C. (1976) Electron-microscopy of membrane-free folded chromosomes from *Escherichia coli*. *Chromosoma 59*, 89–101.
12. Sinden, R. R., and Pettijohn, D. E. (1981) Chromosomes in living *Escherichia coli* cells are segregated into domains of supercoiling. *Proc. Natl. Acad. Sci. U.S.A. 78*, 224–228.
13. Pettijohn, D. E. (1982) Structure and properties of the bacterial nucleoid. *Cell 30*, 667–669.
14. Postow, L., Hardy, C. D., Arsuaga, J., and Cozzarelli, N. R. (2004) Topological domain structure of the *Escherichia coli* chromosome. *Genes Dev. 18*, 1766–1779.
15. Pettijohn, D. E., and Pfenninger, O. (1980) Supercoils in prokaryotic DNA restrained *in vivo*. *Proc. Natl. Acad. Sci. U.S.A. 77*, 1331–1335.
16. Bliska, J. B., and Cozzarelli, N. R. (1987) Use of site-specific recombination as a probe of DNA-structure and metabolism *in vivo*. *J. Mol. Biol. 194*, 205–218.
17. Rice, P. A., Yang, S. W., Mizuuchi, K., and Nash, H. A. (1996) Crystal structure of an IHF-DNA complex: A protein-induced DNA U-turn. *Cell 87*, 1295–1306.
18. Tanaka, I., Appelt, K., Dijk, J., White, S. W., and Wilson, K. S. (1984) 3-Å resolution structure of a protein with histone-like properties in prokaryotes. *Nature 310*, 376–381.
19. Oberto, J., Drlica, K., and Rouviere-Yaniv, J. (1994) Histones, Hmg, Hu, Ihf-Même combat. *Biochimie 76*, 901–908.
20. Swinger, K. K., Lemberg, K. M., Zhang, Y., and Rice, P. A. (2003) Flexible DNA bending in HU-DNA cocrystal structures. *EMBO J. 22*, 3749–3760.
21. Swinger, K. K., and Rice, P. A. (2004) IHF and HU: Flexible architects of bent DNA. *Curr. Opin. Struct. Biol. 14*, 28–35.
22. Friedman, D. I. (1988) Integration host factor: A protein for all reasons. *Cell 55*, 545–554.
23. Freundlich, M., Ramani, N., Mathew, E., Sirko, A., and Tsui, P. (1992) The role of integration host factor in gene-expression in *Escherichia coli*. *Mol. Microbiol. 6*, 2557–2563.
24. Goosen, N., and Vandeputte, P. (1995) The regulation of transcription initiation by integration host factor. *Mol. Microbiol. 16*, 1–7.
25. Wang, S. Q., Cosstick, R., Gardner, J. F., and Gumport, R. I. (1995) The specific binding of *Escherichia coli* integration host factor involves both major and minor grooves of DNA. *Biochemistry 34*, 13082–13090.
26. Goodrich, J. A., Schwartz, M. L., and McClure, W. R. (1990) Searching for and predicting the activity of sites for DNA-binding proteins: Compilation and analysis of the binding sites for *Escherichia coli* integration host factor (IHF). *Nucleic Acids Res. 18*, 4993–5000.
27. Yang, S. W., and Nash, H. A. (1995) Comparison of protein binding to DNA *in vivo* and *in vitro*: Defining an effective intracellular target. *EMBO J. 14*, 6292–6300.
28. Murtin, C., Engelhorn, M., Geiselmann, J., and Boccard, F. (1998) A quantitative UV laser footprinting analysis of the interaction of IHF with specific binding sites: Re-evaluation of the effective concentration of IHF in the cell. *J. Mol. Biol. 284*, 949–961.
29. Ditto, M. D., Roberts, D., and Weisberg, R. A. (1994) Growth-phase variation of integration host factor level in *Escherichia coli*. *J. Bacteriol. 176*, 3738–3748.
30. Azam, T. A., Iwata, A., Nishimura, A., Ueda, S., and Ishihama, A. (1999) Growth phase-dependent variation in protein composition of the *Escherichia coli* nucleoid. *J. Bacteriol. 181*, 6361–6370.

31. Arfin, S. M., Long, A. D., Ito, E. T., Tolleri, L., Riehle, M. M., Paegle, E. S., and Hatfield, G. W. (2000) Global gene expression profiling in *Escherichia coli* K12: The effects of integration host factor. *J. Biol. Chem. 275*, 29672–29684.
32. Ussery, D., Larsen, T. S., Wilkes, K. T., Friis, C., Worning, P., Krogh, A., and Brunak, S. (2001) Genome organisation and chromatin structure in *Escherichia coli*. *Biochimie 83*, 201–212.
33. Ali, B. M. J., Amit, R., Braslavsky, I., Oppenheim, A. B., Gileadi, O., and Stavans, J. (2001) Compaction of single DNA molecules induced by binding of integration host factor (IHF). *Proc. Natl. Acad. Sci. U.S.A. 98*, 10658–10663.
34. Zimmerman, S. B., and Minton, A. P. (1993) Macromolecular crowding: Biochemical, biophysical, and physiological consequences. *Annu. Rev. Biophys. Biomol. Struct. 22*, 27–65.
35. Murphy, L. D., and Zimmerman, S. B. (1994) Macromolecular crowding effects on the interaction of DNA with *Escherichia coli* DNA-binding proteins: A model for bacterial nucleoid stabilization. *Biochim. Biophys. Acta 1219*, 277–284.
36. Zimmerman, S. B., and Murphy, L. D. (1996) Macromolecular crowding and the mandatory condensation of DNA in bacteria. *FEBS Lett. 390*, 245–248.
37. Murphy, L. D., and Zimmerman, S. B. (2001) A limited loss of DNA compaction accompanying the release of cytoplasm from cells of *Escherichia coli*. *J. Struct. Biol. 133*, 75–86.
38. Murphy, L. D., and Zimmerman, S. B. (1997) Stabilization of compact spermidine nucleoids from *Escherichia coli* under crowded conditions: Implications for *in vivo* nucleoid structure. *J. Struct. Biol. 119*, 336–346.
39. Gosule, L. C., and Schellman, J. A. (1978) DNA condensation with polyamines. 1. Spectroscopic studies. *J. Mol. Biol. 121*, 311–326.
40. Chattoraj, D. K., Gosule, L. C., and Schellman, J. A. (1978) DNA condensation with polyamines. 2. Electron-microscopic studies. *J. Mol. Biol. 121*, 327–337.
41. Tabor, C. W., and Tabor, H. (1985) Polyamines in microorganisms. *Microbiol. Rev. 49*, 81–99.
42. Tabor, C. W., and Tabor, H. (1984) Polyamines. *Annu. Rev. Biochem. 53*, 749–790.
43. Nakabachi, A., and Ishikawa, H. (2000) Polyamine composition and expression of genes related to polyamine biosynthesis in an aphid endosymbiont, Buchnera. *Appl. Environ. Microbiol. 66*, 3305–3309.
44. Kornberg, T., Lockwood, A., and Worcel, A. (1974) Replication of *Escherichia coli* chromosome with a soluble enzyme-system. *Proc. Natl. Acad. Sci. U.S.A. 71*, 3189–3193.
45. Murphy, L. D., and Zimmerman, S. B. (1995) Condensation and cohesion of λ-DNA in cell extracts and other media: Implications for the structure and function of DNA in prokaryotes. *Biophys. Chem. 57*, 71–92.
46. Zimmerman, S. B. (2006) Shape and compaction of *Escherichia coli* nucleoids. *J. Struct. Biol. 156*, 255–261.
47. Koh, J., Saecker, R. M., and Record, M. T., Jr. (2008) DNA binding mode transitions of *Escherichia coli* HU$\alpha\beta$: Evidence for formation of a bent DNA−protein complex on intact, linear duplex DNA. *J. Mol. Biol. 383*, 324–346.
48. Kar, S., Edgar, R., and Adhya, S. (2005) Nucleoid remodeling by an altered HU protein: Reorganization of the transcription program. *Proc. Natl. Acad. Sci. U.S.A. 102*, 16397–16402.
49. Sarkar, T., Vitoc, I., Mukerji, I., and Hud, N. V. (2007) Bacterial protein HU dictates the morphology of DNA condensates produced by crowding agents and polyamines. *Nucleic Acids Res. 35*, 951–961.
50. Filutowicz, M., Grimek, H., and Appelt, K. (1994) Purification of the *Escherichia coli* integration host factor (IHF) in one chromatographic step. *Gene 147*, 149–150.
51. Wang, S., Cosstick, R., Gardner, J. F., and Gumport, R. I. (1995) The specific binding of *Escherichia coli* integration host factor involves both major and minor grooves of DNA. *Biochem. Cell Biol. 34*, 13082–13090.
52. Locker, C. R., and Harvey, S. C. (2006) A model for viral geome packing. *Multiscale Model. Simul. 5*, 1264–1279.
53. Petrov, A. S., and Harvey, S. C. (2007) Structural and thermodynamic principles of viral packaging. *Structure 15*, 21–27.
54. Tzlil, S., Kindt, J. T., Gelbart, W. M., and Ben-Shaul, A. (2003) Forces and pressures in DNA packaging and release from viral capsids. *Biophys. J. 84*, 1616–1627.
55. Rau, D. C., and Parsegian, V. A. (1992) Direct measurment of the intermolecular forces between counterion-condenced DNA double helixes. Evidence for long-range attractive hydration forces. *Biophys. J. 61*, 246–259.
56. Berendsen, H. J. C., Postma, J. P. M., Vangunsteren, W. F., Dinola, A., and Haak, J. R. (1984) Molecular dynamics with coupling to an external bath. *J. Chem. Phys. 81*, 3684–3690.
57. Tan, R. K.-Z., Petrov, A. S., and Harvey, S. C. (2006) YUP: A molecular simulation program for coarse-grained and multiscaled models. *J. Chem. Theory Comput. 2*, 529–540.
58. Gosule, L. C., and Schellman, J. A. (1976) Compact form of DNA induced by spermidine. *Nature 259*, 333–335.
59. Bloomfield, V. (1997) DNA condensation by multivalent cations. *Biopolymers 44*, 269–282.
60. Hud, N. V., and Vilfan, I. D. (2005) Toroidal DNA condensates: Unraveling the fine structure and the role of nucleation in determining size in vitro. *Annu. Rev. Biophys. Biomol. Struct. 34*, 295–318.
61. Holmes, V. F., and Cozzarelli, N. R. (2000) Closing the ring: Links between SMC proteins and chromosome partitioning, condensation, and supercoiling. *Proc. Natl. Acad. Sci. U.S.A. 97*, 1322–1324.
62. Vilfan, I. D., Conwell, C. C., Sarkar, T., and Hud, N. V. (2006) Time study of DNA condensate morphology: Implications regarding the nucleation, growth, and equilibrium populations of toroids and rods. *Biochemistry 45*, 8174–8183.
63. Bloomfield, V. A. (1991) Condensation of DNA by multivalent cations: Considerations on mechanism. *Biopolymers 31*, 1471–1481.
64. Lang, D. (1973) Regular superstructures of purified DNA in ethanolic solutions. *J. Mol. Biol. 78*, 247–254.
65. Lang, D., Taylor, T. N., Dobyan, D. C., and Gray, D. M. (1976) Dehydrated circular DNA: Electron microscopy of ethanol-condensed molecules. *J. Mol. Biol. 106*, 97–107.
66. Eickbush, T., and Moudrianakis, E. (1978) The compaction of DNA helices into either continuous supercoils or folded-fiber rods and toroids. *Cell 13*, 295–306.
67. Arscott, P. G., Li, A. Z., and Bloomfield, V. A. (1990) Condensation of DNA by trivalent cations. 1. Effects of DNA length and topology on the size and shape of condensed particles. *Biopolymers 30*, 619–630.
68. Arscott, P. G., Ma, C. L., Wenner, J. R., and Bloomfield, V. A. (1995) DNA condensation by cobalt hexaammine(III) in alcohol-water mixtures: Dielectric constant and other solvent effects. *Biopolymers 36*, 345–364.
69. Plum, G. E., Arscott, P. G., and Bloomfield, V. A. (1990) Condensation of DNA by trivalent cations. 2. Effects of cation structure. *Biopolymers 30*, 631–643.
70. Higgins, N. P., Deng, S., Pang, Z., Stein, R., Champion, K., and Manna, D. (2005) Domain Behavior and Supercoil Dynamics in Bacterial Chromosomes. In *The Bacterial Chromosome* (Higgins, N. P., Ed.) pp 133−153, ASM Press,Washington, DC.
71. Higgins, N. P., Yang, X. L., Fu, Q. Q., and Roth, J. R. (1996) Surveying a supercoil domain by using the gamma delta resolution system in *Salmonella typhimurium*. *J. Bacteriol. 178*, 2825–2835.
72. Borgnia, M. J., Subramaniam, S., and Milne, J. L. S. (2008) Three-dimensional imaging of the highly bent architecture of *Bdellovibrio bacteriovorus* by using cryo-electron tomography. *J. Bacteriol. 190*, 2588–2596.
73. Eltsov, M., and Zuber, B. (2006) Transmission electron microscopy of the bacterial nucleoid. *J. Struct. Biol. 156*, 246–254.
74. Eltsov, M., and Dubochet, J. (2006) Study of the *Deinococcus radiodurans* nucleoid by cryoelectron microscopy of vitreous sections: Supplementary comments. *J. Bacteriol. 188*, 6053–6058.
75. Rubin, R. L. (1977) Spermidine deoxyribonucleic acid interaction *in vitro* and in *Escherichia coli*. *J. Bacteriol. 129*, 916–925.
76. Frenkiel-Krispin, D., Levin-Zaidman, S., Shimoni, E., Wolf, S. G., Wachtel, E. J., Arad, T., Finkel, S. E., Kolter, R., and Minsky, A. (2001) Regulated phase transitions of bacterial chromatin: A non-enzymatic pathway for generic DNA protection. *EMBO J. 20*, 1184–1191.
77. Minsky, A., and Kolter, R. (2005) Stationary-phase chromosomes. In *The bacterial chromosome* (Higgins, N. P., Ed.) pp 155−176, ASM Press, Washington, DC.
78. Eltsov, M., and Dubochet, J. (2005) Fine structure of the *Deinococcus radiodurans* nucleoid revealed by cryoelectron microscopy of vitreous sections. *J. Bacteriol. 187*, 8047–8054.
79. Wolf, S. G., Frenkiel, D., Arad, T., Finkel, S. E., Kolter, R., and Minsky, A. (1999) DNA protection by stress-induced biocrystallization. *Nature 400*, 83–85.

BI8019965